Title

THE ELECTRONIC STRUCTURE OF FbSe AND PbTe I. BAND STRUCTURES, DENSITIES OF STATES AMD EFFECTIVE MASSES

Authors

Martinez, G.
Schluter, M.
Cohen, Marvin L.

Publication Date

1974-11-01

Submitted to Physical Review

LBL-3536
Preprint c.1

THE ELECTRONIC STRUCTURE OF PbSe AND PbTe I. BAND STRUCTURES, DENSITIES OF STATES AND EFFECTIVE MASSES

G. Martinez, M. Schluter, and Marvin L. Cohen

November, 1974

Prepared for the U. S. Atomic Energy Commission
under Contract W-7405-ENG-48

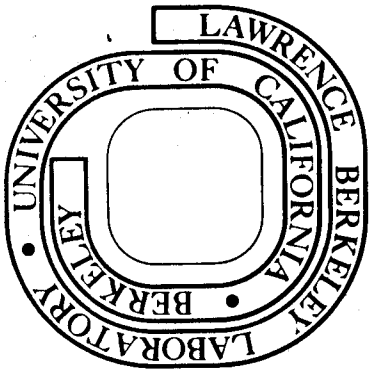

DISCLAIMER

The Electronic Structure of PbSe and PbTe*

I. Band Structures, Densities of States and Effective Masses

G. Martinez†, M. Schlüter‡ and Marvin L. Cohen

Department of Physics, University of California and

Inorganic Materials Research Division,

Lawrence Berkeley Laboratory, Berkeley, California 94720

Abstract

We present new improved pseudopotential calculations for PbSe and PbTe using several non-local corrections in addition to the local empirical pseudopotential. We discuss results for effective masses, Knight shift measurements and recent photoemission measurements. In addition to the optical properties in an energy range from 0 to 20 eV (which will be discussed in a subsequent paper), all the above experimental results can for the first time be explained consistently using one band structure model.

Introduction

A large number of band structures of the lead chalcogenides have already been calculated, using various methods. The OPW method has been employed by F. Hermann et al.,[1] the APW method by several authors[2,3,4] and the KKR method by H. Overhof and V. Rössler.[5] Two different versions of the pseudopotential method have also been published; one of

them including a strong non local s-like potential[6,7] -- of the Lin-Kleinman form and one being purely local -- the empirical pseudopotential method (EPM).[8] None of these calculations was able to give an overall coherent picture of the physical properties of PbSe and PbTe. In particular, only Bernick and Kleinman[7] were able to reproduce the effective masses, whereas only the EPM[8] results yielded optical results in agreement with experiment. Furthermore, the appearance of recent XPS and UPS measurements[9,10] revealed general disagreements with all published band structures. We have thus reopened this problem in an attempt to obtain acceptable agreement with all known experimental measurements.

To perform the calculations we have chosen the EPM which uses a local empirical pseudopotential. This local potential had to be modified by adding an effective mass to the kinetic energy operator and by adding a full non-local d-potential. A detailed description of this procedure is given in Section I. The resulting band structures are presented in Section II together with a justification of the form of the potential used and a discussion of the parameters involved. In Section III we compare the physical properties near the fundamental absorption edge to experimental results. Section IV is devoted to the calculation of the density of states of the valence bands and to a comparison of these results with experimental photoemission data. The study of the optical properties in an energy

range from 0 to 20 eV will be presented in a subsequent paper.[11]

I. Band Structure Calculations

The band structure calculations were done using the empirical pseudopotential method (EPM). This approach is well established and discussed extensively in the literature.[12] Briefly the method involves the solution of a pseudopotential Hamiltonian

$$H = -\Delta + V_L(\underset{\sim}{r}) + V_{NL}(\underset{\sim}{r}) \qquad (1)$$

whose local pseudopotential $V_L(\underset{\sim}{r})$ is expanded in the reciprocal lattice

$$V_L(\underset{\sim}{r}) = \sum_{\underset{\sim}{G}} V(\underset{\sim}{G}) e^{i\underset{\sim}{G}\cdot\underset{\sim}{r}} \qquad (2)$$

where $\underset{\sim}{G}$ is a reciprocal lattice vector. For the case of crystals with rocksalt structure $V(\underset{\sim}{G})$ can be divided into symmetric and antisymmetric contributions

$$V(\underset{\sim}{G}) = V_S(|\underset{\sim}{G}|)\cdot S_S(\underset{\sim}{G}) + V_A(|\underset{\sim}{G}|)\cdot S_A(\underset{\sim}{G}) \qquad (3)$$

where V_S and V_A, the symmetric and antisymmetric form factors are treated as empirical parameters. They are related to the atomic form factors V_c and V_a of cation and anion by

$$V_S = \frac{V_c + V_a}{2} \quad \text{and} \quad V_A = \frac{V_c - V_a}{2} \quad . \qquad (4)$$

S_S and S_A denote the corresponding symmetric and antisymmetric structure factors. The non-local potential $V_{NL}(r)$ in Eq. (1) contains two different contributions:

a) a non-local and (generally energy dependent) correction W to the local atomic pseudopotential V_L as derived e.g. from the usual OPW formalism[13] and

b) a relativistic correction R which describes the spin-orbit interaction. Only the spin-orbit interaction part of the relativistic correction is added explicitly for this interaction breaks the symmetry of the non-relativistic Hamiltonian. Other relativistic terms have full symmetry and can be considered to be absorbed into the non-relativistic empirical pseudopotential.

In the usual plane wave representation, the non-local, energy dependent pseudopotential becomes formally $W(\underset{\sim}{k}+\underset{\sim}{G}, \underset{\sim}{k}+\underset{\sim}{G}', E)$. It is believed that the first order influence on the band structure of W can be accounted for by retaining only main-diagonal terms i.e. terms with $\underset{\sim}{G} = \underset{\sim}{G}'$. Moreover, it has been shown[12] that in this case nonlocality and energy dependence can be simulated by the introduction of an effective mass $m^* = m_K \cdot m_E$. In terms of $W(\underset{\sim}{K},\underset{\sim}{K},E)$ m_K and m_E can be expressed as

$$m_K^{-1} = 1 + \frac{1}{|\underset{\sim}{K}|} \frac{\partial W}{\partial k}$$

$$m_E = 1 - \frac{\partial W}{\partial E} \qquad (5)$$

where the derivatives are usually taken at the Fermi level. In an actual band structure calculation m^* can either be treated as an empirical parameter or it can be calculated from non-local atomic model potentials.[14] In the latter

case the value of m* entering the crystal Hamiltonian has to be computed according to the linear additive behavior of W for different atoms. Even though this effective mass treatment appears to be a very crude approximation to the "true" non-locality it nevertheless simulates s-p non-locality to some extent. Since 1/m* scales the kinetic energy, it influences the energy separation of the low-lying (s-like) states differently from the higher lying (mostly p- and d-like) states. It follows from the different localization of non-local potentials in K-space (we shall discuss this point in Section III) that retaining only main-diagonal terms of W is a better approximation for s-p non-locality than it is for d-non-locality. It seems therefore desirable to include d-non-locality in a more explicit way, e.g. by retaining off-diagonal terms of W as well.

A typical form for the d-like non-local potential can be obtained from the original OPW Hamiltonian

$$\langle \underset{\sim}{k}+\underset{\sim}{G}|W_i^d|\underset{\sim}{k}+\underset{\sim}{G}'\rangle = A_i\langle \underset{\sim}{K}|t_i\rangle\langle t_i|\underset{\sim}{K}'\rangle \qquad (6)$$

where $\underset{\sim}{K} = \underset{\sim}{k}+\underset{\sim}{G}$ and where $|t_i\rangle$ should include all d-like core states of atoms of type i. In practice, however, only d-like states of the last filled core shell have to be considered since the overlap matrix elements in (6) decrease by about one order of magnitude with each core shell. The simulation of d-like non-local potentials using Eq. (6) introduces one additional parameter for each kind of atom.

The integrals in Eq. (6) can be evaluated by taking atomic core wavefunctions[15] $R_{n\ell}(r)$; Eq. (6) then becomes

$$\langle \underset{\sim}{k}+\underset{\sim}{G}|w_i^d|\underset{\sim}{k}+\underset{\sim}{G}'\rangle = A_i \frac{4\pi(2\ell+1)}{\Omega_0} P_\ell(\cos\alpha)$$

$$\times B^i_{n\ell}(|\underset{\sim}{K}|)\, B^i_{n\ell}(|\underset{\sim}{K}'|)\; S_i(\underset{\sim}{G}'-\underset{\sim}{G}) \quad \ell = 2 \qquad (7)$$

where Ω_0 denotes the unit cell volume, P_ℓ a Legendre polynomial, and α the angle between $\underset{\sim}{k}+\underset{\sim}{G}$ and $\underset{\sim}{k}+\underset{\sim}{G}'$. $S_i(\underset{\sim}{G}'-\underset{\sim}{G})$ represents the usual structure factor for atoms of type i and $B^i_{n\ell}(|\underset{\sim}{K}|) = \int_0^\infty R^i_{n\ell} j_\ell(|\underset{\sim}{K}|r) r^2 dr$ is a slowly varying function of $|\underset{\sim}{K}|$, depending on atomic radial functions $R^i_{n\ell}$ and on spherical Bessel functions j_ℓ.

The non-local relativistic correction R can be derived from a spin-orbit Hamiltonian of the form

$$H_{so} = \frac{\hbar}{4m^2c^2} [\nabla V(\underset{\sim}{r}) \times \underset{\sim}{p}]\cdot\underset{\sim}{\sigma} \qquad (8)$$

where $V(\underset{\sim}{r})$ is the real crystal potential, $\underset{\sim}{p}$ is the momentum operator, and $\underset{\sim}{\sigma}$ is the Pauli spin operator. Following a procedure described by Weisz[16] we can derive the following matrix element appearing in the pseudopotential Hamiltonian:

$$R(\underset{\sim}{K}',\underset{\sim}{s}';\underset{\sim}{K},\underset{\sim}{s}) = \sum_i \underset{\sim}{\sigma}_{s',s} (\Lambda_p{}^i + \Lambda_d{}^i)\; S_i(\underset{\sim}{K}-\underset{\sim}{K}') \qquad (9)$$

where S_i are atomic structure factors and $\underset{\sim}{\sigma}_{s',s} = \langle s'|\underset{\sim}{\sigma}|s\rangle$ are matrix elements in spin space. The non-local potentials

$$\Lambda_p{}^i = 12\pi \frac{-i\lambda_p{}^i}{\Omega_0} B^i_{n,1}(|\underset{\sim}{K}|)\, B^i_{n,1}(|\underset{\sim}{K}'|)\; \frac{[\underset{\sim}{K}'\times\underset{\sim}{K}]}{|\underset{\sim}{K}|\,|\underset{\sim}{K}'|} \qquad (10)$$

$$\Lambda_d{}^i = 60\pi \frac{-i\lambda_d{}^i}{\Omega_0} B^i_{n,2}(|\underset{\sim}{K}|)\, B^i_{n,2}(|\underset{\sim}{K}'|)\; \frac{[\underset{\sim}{K}'\times\underset{\sim}{K}]\cdot[\underset{\sim}{K}'\cdot\underset{\sim}{K}]}{|\underset{\sim}{K}|^2\,|\underset{\sim}{K}'|^2}$$

represent the core spin-orbit interaction projected on the valence pseudo wavefunction. Non-locality enters Eq. (10) via the vector product $[\underset{\sim}{K}'\times\underset{\sim}{K}]$ for the p-like contribution and via $[\underset{\sim}{K}'\times\underset{\sim}{K}]\cdot[\underset{\sim}{K}'\cdot\underset{\sim}{K}]$ for the d-like contribution. This reflects the different angular behavior of p- and d-functions. The functions $B^{i}_{n,\ell}(|\underset{\sim}{K}|)$ are the radial integrals which appeared in Eq. (7).

As mentioned in the discussion of Eq. (6), only the outermost core shell has to be considered in the calculation of the overlap integrals. The empirical parameters $\lambda_p{}^{i}$, $\lambda_d{}^{i}$ determine the strength of the spin-orbit coupling in the crystal. With the assumption that the ratio of these parameters for different atoms i in the crystal is the same as for the free atoms we end up with two parameters λ_p and λ_d describing the spin-orbit interaction in the crystal.

II. Results for the Band Structures and Discussion of Important Parameters

The parameters used in our band structure calculations are presented in table 1. The resulting $E(\underset{\sim}{k})$ curves are shown in Fig. 1 for PbSe and in Fig. 2 for PbTe.

The lattice parameter a has been taken from x-ray measurements at 4°K for PbTe[17] and has been computed from the experimental dilation coefficient as a function of temperature[18] together with the room temperature value of the lattice constant for PbSe.[17]

For reasons of computation the local pseudopotentials have to be cut off at some finite $|\underset{\sim}{G}|$ value. It is generally believed that the effect of this truncation can be absorbed by the remaining pseudopotential form factors. This argument can be accepted if, in first order, the influence of the higher $|\underset{\sim}{G}|$ form-factors on the different electronic levels is either small or at most of the same order of magnitude as the influence of the lower $|\underset{\sim}{G}|$ form factors. We therefore have computed the derivatives of the most important gaps with respect to $|\underset{\sim}{G}|$ form factors until $G^2 = 27$, for some selected $\underset{\sim}{k}$ points. Though the convergence, up to this value, becomes relatively poor (~0.2 eV) we find that the assumptions made above are acceptable for the valence bands, but become generally poorer for the conduction bands and are especially bad for the d levels within the conduction bands. For example, if we are looking at the relative energy separation ΔE between the lowest X_7^+ level, which is of pure d-character, and the top for the valence band, and if we restrict ourselves to a constant value of the fundamental gap, we find the following derivatives with respect to different form factors:

$$\frac{\partial \Delta E}{\partial V_{24}} \sim -35 \; ; \quad \frac{\partial \Delta E}{\partial V_4} \sim -10 \; ; \quad \frac{\partial \Delta E}{\partial V_8} \sim -1.6 \; .$$

In view of these results, we can believe that cutting off the local pseudopotential at some $|\underset{\sim}{G}|^2 < 24$, affects the band structure like a non-local <u>d-like</u> potential. It depends solely on the remaining local form factors whether this spurious non-local potential is attractive or repulsive.

For our calculation we choose a cut-off at $G^2 = 16$ which leads to an energy convergence of better than 0.025 eV. The lead potentials used in both salts are very similar which is consistent with the fact that we do not expect a large difference in the screening between PbSe and PbTe. Comparing our cation and anion potentials, their difference in electronegativity is generally smaller than that reported in earlier publications.[8] This results in a decrease of the gap between the two low lying valence s-bands which is, as we shall see in Section V, in accordance with recent XPS and UPS data.

The effective mass parameters have been chosen empirically. However, since these values should not depend on the particular screening, we expect them to be close to the values calculated from atomic model potentials. Appapillai and Heine[14] have recently calculated optimized model potentials and effective masses for a number of atoms including Pb, Se and Te. They find the following masses: for Pb $m_k = 0.917$, $m_E = 0.963$; for Se, $m_k = 1.0002$, $m_E = 0.975$; and for Te, $m_k = 1.02$, $m_E = 0.969$. The corresponding effective masses for the compounds can be computed according to Eq. (5). Thus in the case of PbTe for example we find:

$$m_k^{-1}(\mathrm{PbTe}) = 1 + (m_k^{-1}(\mathrm{Pb})-1) + (m_k^{-1}(\mathrm{Te})-1) \text{ and}$$
$$m_E(\mathrm{PbTe}) = 1 + (m_E(\mathrm{Pb})-1) + (m_E(\mathrm{Te})-1)$$

From that we obtain the following values:

$m_k(PbTe) = 0.934$; $m_E(PbTe) = 0.932$; $m^*(PbTe) = 0.870$

$m_k(PbSe) = 0.917$; $m_E(PbSe) = 0.944$; $m^*(PbSe) = 0.866$

Considering the uncertainty involved in this kind of calculations which is essentially given by the inaccurate determination of the energy slope of the model potential parameters, we can say that these values are in good agreement with our empirical findings (see Table 1).

We shall now discuss in more detail the influence of the use of effective masses on the band structure results. The concept of introducing effective masses is to reproduce non-locality at $\underset{\sim}{G} = 0$, which is equivalent to consider only main-diagonal matrix elements of the non-local potential. The validity of this approach, however, demands that the off diagonal terms have to be small compared to the diagonal terms. In other words one has to assume that in Eq. (6), $|\langle \underset{\sim}{K}|t\rangle|^2$ is smaller than $\langle \underset{\sim}{K}|t\rangle\langle t|\underset{\sim}{K}+\underset{\sim}{G}'\rangle$ for most of the $\underset{\sim}{G}'$-vectors (we have set $\underset{\sim}{k}+\underset{\sim}{G} = \underset{\sim}{K}$). This turns out to be a reasonable assumption for s and p states but it becomes questionable for d states. This results from the extension in $\underset{\sim}{K}$ space of the matrix element $\langle \underset{\sim}{K}|t\rangle$. For a mean value of $|\underset{\sim}{K}|$ (such as $\underset{\sim}{K}^2 = 8$), $\langle \underset{\sim}{K}|t\rangle$ is still an increasing function of $|\underset{\sim}{K}|$ for d-states and in some cases the off-diagonal terms are even bigger than the diagonal terms. The effective mass approach therefore does not seem to be a sufficiently accurate treatment for d non-locality.[19]

This fact, together with the remarks concerning the cut off of the local pseudopotential, justifies the inclusion of a complete non-local d_{Λ}-like potential into the calculation of the band structures. However, the repulsive or attractive character of this potential can only have a relative meaning with respect to the local, empirical potentials which we used. For this reason we shall not try to attribute any physical meaning to the fact that we used an attractive potential for lead (for PbTe) and a repulsive one for selenium (for PbSe). In Table 1 we give the values A_i according to Eq. (7) for the non local pseudopotentials used in our calculations. These values might at first sight appear to be very large. However, to compare them with the local form factors, they have to be corrected by several factors arising from the functions $B^i_{n\ell}$ in Eq. (7) and from the volume Ω_0. The comparable values are thus -0.0044 ryd for PbTe and +0.0019 ryd for PbSe. Compared to the local pseudopotential, these values are quite small as they should be if they are to remain a small correction to the basic local scheme. The influence on the band structure of these connections is essential only to reproduce the optical properties of these two compounds above 6 eV. This will be discussed in detail in a subsequent paper.[11] We should add on this particular point, that all the arguments given here to support the introduction of a non local d-like potential are quite general and should be

valid for most semiconductors. Although for some cases, the introduction of an effective mass is not justified, e.g. Si where theoretically $m^* = 0.999$,[14] there still remains the cut off of the local pseudopotential, which should by itself justify the use of a non local d-like potential.

Though Si calculations,[13] performed without a non local d-like potential, have succeeded to reproduce the optical properties for energies up to 6 eV, the d-like potential might be necessary to reproduce the optical properties at higher energies. Furthermore our arguments do not exclude a case in which the cut-off of the higher $|\underset{\sim}{G}|$ form factors can accidentally be absorbed by the remaining form factors.

The spin-orbit parameters have also been chosen empirically in such a way that the splitting of $\Gamma_6^- - \Gamma_8^-$ of the upper valence bands correspond to that found by the OPW method.[1] As inferred from atomic values the d contribution to the spin-orbit splitting is quite negligible and can be left out to simplify the calculations.

III. Effective masses

The lead salts exhibit a small direct gap at the point L of the Brillouin zone. It is known that the properties connected with this gap can only be explained by taking into account the mass anisotropy and the strong non-parabolicity of the bands around the gap energy. In the following we

shall discuss only the effect of anisotropy. For this discussion it is essential to know the values of the effective masses at L. The experimental values are given in Table 2 for PbSe and PbTe.[20] The most striking feature seems to be the large difference in the anisotropy of the masses for longitudinal (parallel to ΓL) and transverse (perpendicular to the ΓL) direction between the two salts. It is known[21,22] that a $\underset{\sim}{k}\cdot\underset{\sim}{p}$ theory around L, including only six bands can reproduce quite well the band structure and the associated physics in this energy range. On the basis of this theory we expect, owing to the large difference in the mass anisotropy between PbSe and PbTe, a noticeable change in the bands around the L point. Bernick and Kleinman[7] were the first to propose an inversion of the two L_6^- levels forming the first two conduction bands going from PbSe to PbTe. The reason for this can be understood in the $\underset{\sim}{k}\cdot\underset{\sim}{p}$ framework, if we write down the expression for the effective masses and look at the origin of the six bands in a scheme without spin-orbit interaction (Fig. 3). Without spin-orbit interaction there remain only four bands and the $\underset{\sim}{p}$-matrix elements which couple these bands have well defined polarizations ($\perp$ and $\parallel$) as shown in Fig. 3. It turns out from actual calculations that $P_{13}^{\perp}$ or $P_{31}^{\perp}$ are larger than $P_{11}^{\parallel}$ by about a factor of 3. Thus, if the lowest L_6^- level originates from L_2^- we expect, owing to the difference between the relative energies, a compensation for the difference in the

values of the matrix elements for the two polarizations and consequently a relatively weak mass anisotropy. This should clearly be the PbSe case. On the other hand, if the lowest L_6^- level originates from an L_3^- level, we expect an accumulative effect and longitudinal masses much larger than the transverse ones. This is the case for PbTe.

We found in this framework that this band ordering represents the only solution which can explain the very different experimentally observed anisotropies and that this solution does not bring about any contradiction in any of the observed properties of these compounds. In particular we shall show in a later publication[23] that with this particular ordering the pressure dependence of the gap can be well understood. The calculated effective masses at L are given for comparison in Table 2. They have been calculated by fitting a parabola very close to the L point (in the longitudinal and in the transverse direction) in the band structure. This procedure appears to be necessary to obtain accurate masses because the values of the matrix elements are known only within an error of about 10%. Due to the particular structure of the expression for the effective masses in the $\underset{\sim}{k}\cdot\underset{\sim}{p}$ theory, any error in the matrix elements connecting the two levels at the gap is considerably enhanced by the small value of this gap, thus strongly affecting the values of the effective masses.

IV. Knight Shift Experiments

Knight shift measurements on Pb^{207} in PbSe and PbTe have been reported[25] recently. Their interpretation provides a very useful quantity, namely the relative charge density at the lead site $|\psi(0)|^2$ for the upper valence band at L (the experiments were done with p-type material). Due to the relatively large uncertainties involved in the determination of the g-factors, the values deduced for $|\psi(0)|^2$ are known only within ±10%. Within this uncertainty, the ratio of $|\psi(0)|^2$ at the lead atom, normalized to the volume of the primitive cell, is found to be equal for both salts and about 0.67.

$|\psi(0)|^2$ corresponds essentially to the s-like part of the wavefunction around the lead atoms at the top of the valence band. To evaluate this quantity we have expanded the plane wave solutions of our EPM calculations in spherical harmonics. Then

$$\psi(\underset{\sim}{r}) = \sum_{\ell=0}^{L} \psi_\ell(\underset{\sim}{r}) \quad . \tag{11}$$

The sum in Eq. (11) was restricted to L = 2 and all functions are normalized neglecting higher angular momenta. Then the ℓ character, $c^\ell = \langle \psi_\ell | \psi_\ell \rangle$, of the wavefunction can be characterized by

$$c^\ell = 4\pi \sum_{\underset{\sim}{G},\underset{\sim}{G}'} a_{\underset{\sim}{G}}^* a_{\underset{\sim}{G}'} (2\ell+1) P_\ell(\cos\alpha) \times \int_0^{R_\ell} j_\ell(|\underset{\sim}{G}+\underset{\sim}{k}|\, r) j_\ell(|\underset{\sim}{G}'+\underset{\sim}{k}|\, r) r^2 dr \tag{12}$$

where P_ℓ is the Legendre polynomial, α is the angle between $\underset{\sim}{K} = \underset{\sim}{G}+\underset{\sim}{k}$ and $\underset{\sim}{K}' = \underset{\sim}{G}'+\underset{\sim}{k}$, and $j_\ell(x)$ the spherical Bessel function of order ℓ. The coefficients $a_{\underset{\sim}{G}}$ are the eigensolutions of the EPM calculation. R_ℓ is the radius of a sphere around the atom under consideration in which we evaluate the charge density. The integration in (11) can be carried out analytically for all ℓ. Here we are interested in the $\ell=0$ case (s character) only. In this case we obtain

$$c^0 = 4\pi \sum_{\underset{\sim}{G},\underset{\sim}{G}'} a_{\underset{\sim}{G}}^* a_{\underset{\sim}{G}'} \times \frac{1}{|\underset{\sim}{K}|^2 \cdot |\underset{\sim}{K}'|^2} \left(\frac{\sin(|\underset{\sim}{K}|R)\cos(|\underset{\sim}{K}'|R)}{|\underset{\sim}{K}|} - \frac{\sin(|\underset{\sim}{K}'|R)\cos(|\underset{\sim}{K}|R)}{|\underset{\sim}{K}'|} \right) \quad \text{for } |\underset{\sim}{K}| \neq |\underset{\sim}{K}'| \tag{13}$$

$$\times \frac{1}{2|\underset{\sim}{K}|^3} (|\underset{\sim}{K}|R - \sin(|\underset{\sim}{K}|R)\cos(|\underset{\sim}{K}|R)) \quad \text{for } |\underset{\sim}{K}| = |\underset{\sim}{K}'|$$

Clearly this quantity depends on the value chosen for R. It turns out that c^0 normalized to R_0^3 passes through a minimum as a function of R at R = 1.20 Å for PbSe and R = 1.25 Å for PbTe. These values correspond well to the charge contours deduced from charge density plots of the two salts which will be discussed in a later publication.[26]

With these values of R the properly normalized values of c^0 are found to be c^0(PbTe) = 0.61 and c^0(PbSe) = 0.73 around the lead atom for the top most valence band at L. Owing to the aforementioned uncertainties in the experimental results, and to the fact that the calculations were done on

the basis of pseudo wavefunctions, the agreement between theory and experiment is very good.

Another interesting piece of information provided by Knight Shift experiments concerns n-type lead salts. The interpretation of these experiments reveal that the wavefunction of the first conduction band at L must have $p^{1/2}$ character around lead for both compounds.

This is not in contradiction with the fact that the conduction bands have different origins for the two salts. This result is confirmed by our calculations. The information concerning the character of the lowest conduction bands will be very useful in determining the threshold energy for reflectivity measurements in the far UV involving transitions from the lead d-core levels into the conduction bands. Details of these experiments will be presented in a subsequent paper.[11]

V. X-ray (XPS) and Ultraviolet (UPS) Photoemission Experiments

XPS and UPS experiments are believed to afford direct information about the density of states of the valence bands. To calculate the densities of states from our EPM band structures we have used the method of Gillat and Dolling.[27] $\underset{\sim}{K}$-space integration was done on the basis of 207 calculated points in the irreducible part (1/48) of the Brillouin zone. Transition matrix elements and energy gradients were calculated using $\underset{\sim}{k}\cdot\underset{\sim}{p}$ techniques.

The resulting densities of states are presented in the figures 1 and 2. First we notice that the density of states for the Λ conduction bands is very uniform in both salts and thus seems to indicate the free electron-like behavior of these bands. This implication, however, proves to be incorrect as is shown[11] when analyzing the spectra of core- to conduction band transitions where it is found that the conduction band states retain a significant amount of atomic character. As a further overall feature we find the valence bands to be considerably broader in PbSe than in PbTe. We shall now compare our calculations with recently reported XPS[9] and UPS[10] measurements (Figs. 4 and 5). In these figures we have broadened the different groups of valence bands in the calculated curves with different broadening functions in order to facilitate the comparison with experiment. The three upper valence bands (p bands) have been broadened with a characteristic energy of 0.25 eV, the lead s-band with an energy of 0.7 eV and the lowest valence band (anion s band) with an energy of 1 eV. In addition we give in Table 3 a quantitative comparison between our results and the experimental data by assigning the various structures to critical points in $\underset{\sim}{k}$-space. One of the difficulties encountered in the XPS or UPS measurements is to determine reference energies (i.e. the top of the valence bands). The reference energy is in general known only within ±0.4 eV for XPS measurements and ±0.1 eV for UPS measurements. In the figures 4 and 5 we have therefore tried to align

the peak energies of the s-lead bands (2nd valence band) which tends to give better agreement between the peak energies of the p bands of the two experimental curves than the quoted energy zeros. This, however, also shows that the given reference energy for the XPS measurements of PbSe is probably too large by 0.3 eV. On the other hand the two lower peaks in the experimental curves are obtained after subtraction of a large background and therefore could be affected by a possible error exceeding the tolerance of ±0.1 eV given in Ref. (9). Furthermore all results are obtained with an experimental resolution of about 0.5 eV which has to be taken into account in comparing our calculations to experiment. In view of these possible errors, the agreement between theory and both experiments is excellent.

Conclusion

We have presented calculations on the electronic structure of the lead chalcogenides PbSe and PbTe which for the first time are in excellent agreement with existing experimental results. The different anisotropies of the effective masses at the band gap at the point L can be reproduced very accurately and be explained by different band ordering effects. Knight shift data giving information about the character of the wavefunctions at both valence- and conduction band edges can be well understood by analyzing the pseudo-plane waves in terms of angular momentum eigenfunctions. Finally, the calculated density of states for

valence bands is compared with recent XPS and UPS measurements. The agreement is excellent and deviations fall within the experimentally given tolerance. The reproduction of all these experiments as well as of optical measurements in an energy range from 0 to 20 eV, which will be discussed in a subsequent paper, was achieved using empirical, local pseudopotentials combined with an effective mass parameter, simulating s-p non-locality and with a full non-local d-like potential. The latter potential only had to be included to obtain correct reflectivity data for energies above 6 eV.

References

* Supported in part by the National Science Foundation Grant GH 35688.

† On leave from University of Paris VI, France on NATO fellowship. Permanent address: Laboratoire de physique des solides, Université Paris VI, 4 place Jussieu, 75 Paris 5°, France.

‡ Swiss National Science Foundation fellow.

1. F. Herman, R. L. Kortum, I. Ortenburger and J. P. Van Dyke, J. Phys. (Paris) Suppl. 29, C4-62 (1968).

2. L. E. Johnson, J. B. Conklin, Jr. and G. W. Pratt, Jr., Phys. Rev. Lett. 11, 538 (1963), Phys. Rev. 137, A1282 (1965).

3. L. G. Ferreira, Phys. Rev. 137, A1601 (1965).

4. S. Rabii, Phys. Rev. 107, 801 (1958) and Phys. Rev. 173, 918 (1968).

5. H. Overhof and V. Rössler, Phys. Status Solidi 37, 691 (1970).

6. P. J. Lin and L. Kleinman, Phys. Rev. 142, 478 (1966).

7. R. L. Bernick and L. Kleinman, Solid State Comm. 8, 569 (1970).

8. Y. W. Tung and M. L. Cohen, Phys. Rev. 180, 823 (1969), S. E. Kohn, P. Y. Yu, Y. Petroff, Y. R. Shen, Y. Tsang and M. L. Cohen, Phys. Rev. B8, 1477 (1973).

9. F. R. McFeely, S. Kowalczyk, L. Ley, R. A. Pollak and D. A. Shirley, Phys. Rev. B7, 5228 (1973).

10. M. Cardona, D. W. Langer, N. J. Shevchik and J. Tejeda, Phys. Stat. Sol. b58, 127 (1973).

11. G. Martinez, M. Schlüter and M. L. Cohen, to be published.

12. M. L. Cohen and V. Heine in Solid State Physics, edited by H. Ehrenreich, F. Seitz and D. Turnbull (Academic Press, New York, 1970), vol. 24, p. 37.

13. F. Hermann, R. L. Kortum, C. D. Kuglin, J. P. Van Dyke and S. Skillman in Methods in Computational Physics, edited by B. Alder, S. Fernbach and M. Rotenburg (Academic Press, New York, 1968), vol. 8, p. 193 and also references therein.

14. D. Weaire, Proc. Phys. Soc. 92, 956 (1967), and Tables of the Optimized Model Potential in Solids, M. Appapillai and V. Heine, Technical Report No. 5 (1972), Cavendish Laboratory, Cambridge, U.K.

15. F. Herman and S. Skillman in Atomic Structure Calculations, Prentice Hall Inc., Englewood Cliffs, N.J. 1963.

16. G. Weisz, Phys. Rev. 149, 504 (1966).

17. R. W. G. Wyckoff, Crystal Structures, vol. 1, edited by Interscience Pub. (John Wiley & Sons) New York 1963.

18. S. I. Novikova and N. Kh. Abrikosov, Soviet Phys. Solid State 5, 1397 (1964).

19. J. Chelikowsky and M. L. Cohen, Phys. Rev. Lett. 31, 1582 (1973), Phys. Rev. Lett. 32, 674 (1974), Phys. Lett. 47A, 7 (1974).

20. K. F. Cuff, M. R. Ellet, C. D. Kuglin and L. R. Williams, Proc. Int. Conf. Phys. of Semiconductors, p. 677, Dunod, Paris (1964).

21. G. Martinez, Phys. Rev. B8, 4678 (1973).

22. J. Melngailis and T. C. Harman, Phys. Rev. B5, 2250 (1972).

23. G. Martinez, M. Schlüter and M. L. Cohen, to be published.

24. D. L. Mitchell and R. F. Wallis, Phys. Rev. 151, 581 (1966).

25. J. Y. Leloup, B. Sapoval and G. Martinez, Phys. Rev. B7, 5276 (1973).

26. G. Martinez, M. Schlüter and M. L. Cohen, to be published.

27. G. Gillat and G. Dolling, Phys. Lett. 8, 304 (1964).

Table Captions

Table 1. Parameters used in the calculation of the band structures of PbSe and PbTe. The local pseudopotentials symmetric-VS and antisymmetric-VA as well as the non-local parameters A_i entering Eqs. (3) and (7) are given in Rydbergs. For a comparison of local and non-local potentials, the latter have to be scaled by various factors (see text), which decrease them to -0.0044 ryd (for PbTe) and to 0.0019 ryd (for PbSe).

Table 2. Calculated and experimental[20] effective masses for PbSe and PbTe given in units of free electron masses.

Table 3. Comparison of structure in the XPS[9] and UPS[10] data with the calculated density of valence states and assignment to specific points in $\underset{\sim}{k}$-space. The $\underset{\sim}{k}$-point P' has the coordinates (0.71, 0.46, 0). All energies are given in eV and counted from the top of the valence bands. The XPS data on PbSe have been shifted by 0.3 eV towards lower energies to compensate for an error in the location of the Fermi level (see text). The theoretical energies in parenthesis are those obtained after the broadening (see text).

Table 1

	$a(\mathring{A})$ 4°K	VA(3)	VS(4)	VS(8)	VA(11)	VS(12)	VS(16)	m^*/m_0	A_c	A_A
PbSe	6.095	0.059	-0.2064	-0.0129	-0.010	0.040	0.0688	0.85	0	+12.0
PbTe	6.454	0.0358	-0.238	-0.0168	-0.0112	0.0548	0.0668	0.85	-1.	0

Table 2

	PbSe		PbTe	
	Experiment	Calculation	Experiment	Calculation
m_ℓ^v	0.068 ± 0.015	0.083	0.31 ± 0.05	0.265
m_t^v	0.034 ± 0.007	0.030	0.022 ± 0.003	0.0232
m_ℓ^c	0.070 ± 0.015	0.077	0.24 ± 0.05	0.219
m_t^c	0.040 ± 0.008	0.032	0.024 ± 0.003	0.0225

Table 3

	Structures in XPS (Ref. 9) measurements	Structures in UPS (Ref. 10) measurements	Structures in EPM calculations	Assignment
PbTe		-0.65	-0.4(-0.6)	Δ(5),Λ(5)
		-1.1	-0.9(-1.1)	Γ(4,5)
	-2.3	-2.4	-1.8 -2.2 (-2.)	Λ(3) Δ(3),X(5)
			-3.05(-2.9)	X(4)
	-8.20	-8.3	-8.25(-8.0)	Σ(2),L(2)
	-11.7	-12.5	-11.3(-11.6)	X(1),K(1)
PbSe	-0.9	-0.8	-1.0(-0.85)	P'(5)
	-1.90	-2.2	-2.0(-1.90)	Γ(4,5),Λ(4)
			-2.4(-2.30)	Γ(3)
		-3.35	-2.8(-2.80)	Δ(3)
			-3.3(-3.4)	Δ(4),Σ(3)
			-3.8(-4.0)	X(5)
	-8.3	-8.3	-8.4(-8.3)	P'(2),Σ(2)
	-12.6	-13.4	-13.2(-13.5)	X(1),K(1)

Figure Captions

Figure 1. EPM band structure of PbSe along some high symmetry lines in the Brillouin zone. The symmetry notations are those of Ref. (8). The calculated density of states is also given.

Figure 2. EPM band structure of PbTe together with the calculated density of states. The same symmetry notation is used as for Fig. 1.

Figure 3. Band configurations with and without spin orbit interaction around the fundamental absorption edge for PbSe and PbTe. The non-zero matrix elements of the crystal momentum in the absence of spin-orbit coupling are shown schematically for the longitudinal ($\parallel$, i.e. parallel to ΓL) and the transverse direction ($\perp$, i.e. perpendicular to ΓL). The notation is that of Mitchell and Wallis.[24]

Figure 4. XPS[9] (dotted line) and UPS[10] (dashed line) photoemission spectra of the valence band structure of PbTe. Calculated densities of states are superimposed. The calculated curves are convoluted by an energy-dependent broadening function (see text). The peak energies of the lead s-levels at about -8 eV have been aligned to compare the different spectra.

Figure 5. XPS and UPS for PbSe; see caption of Figure 4.

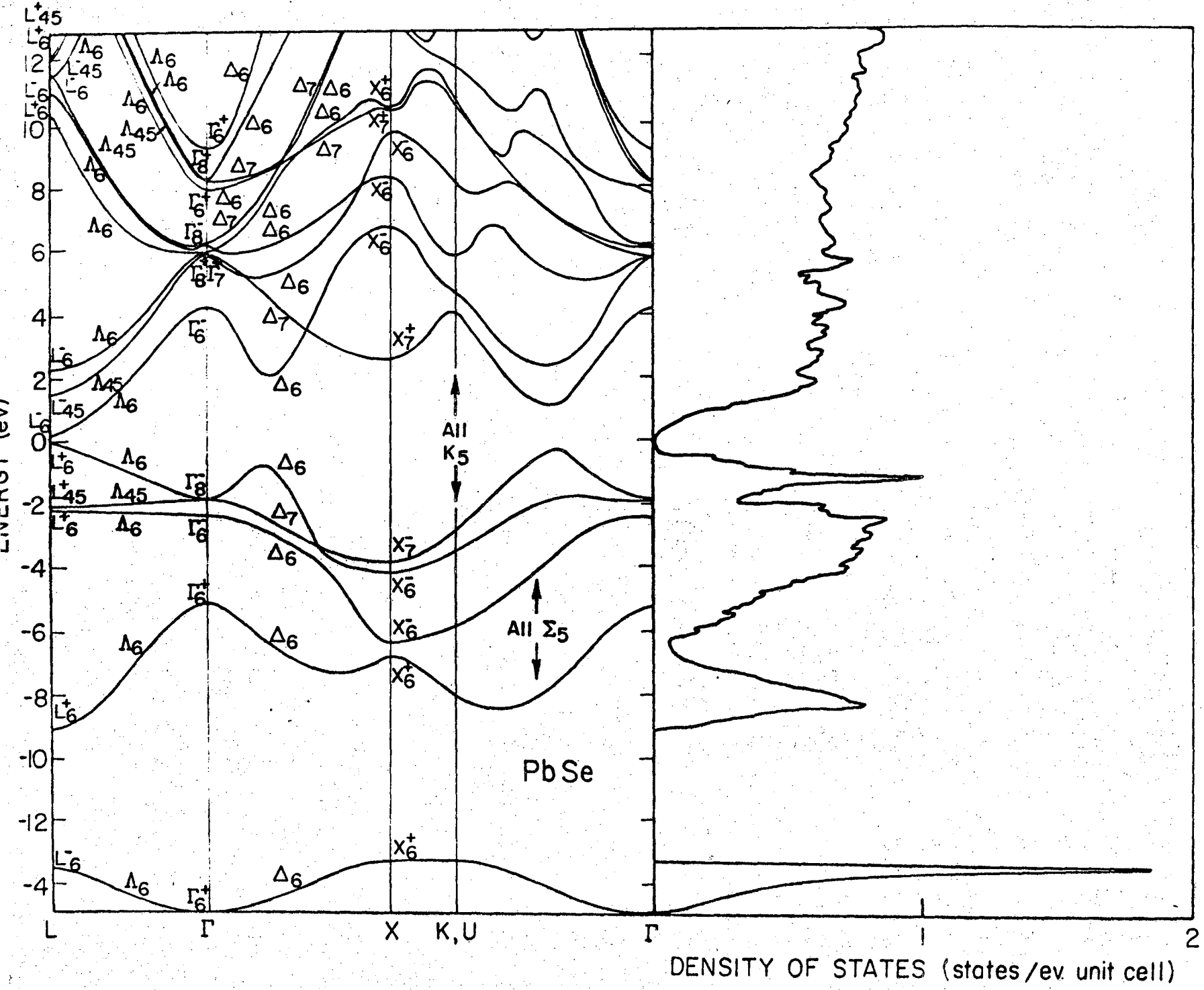

Figure 1

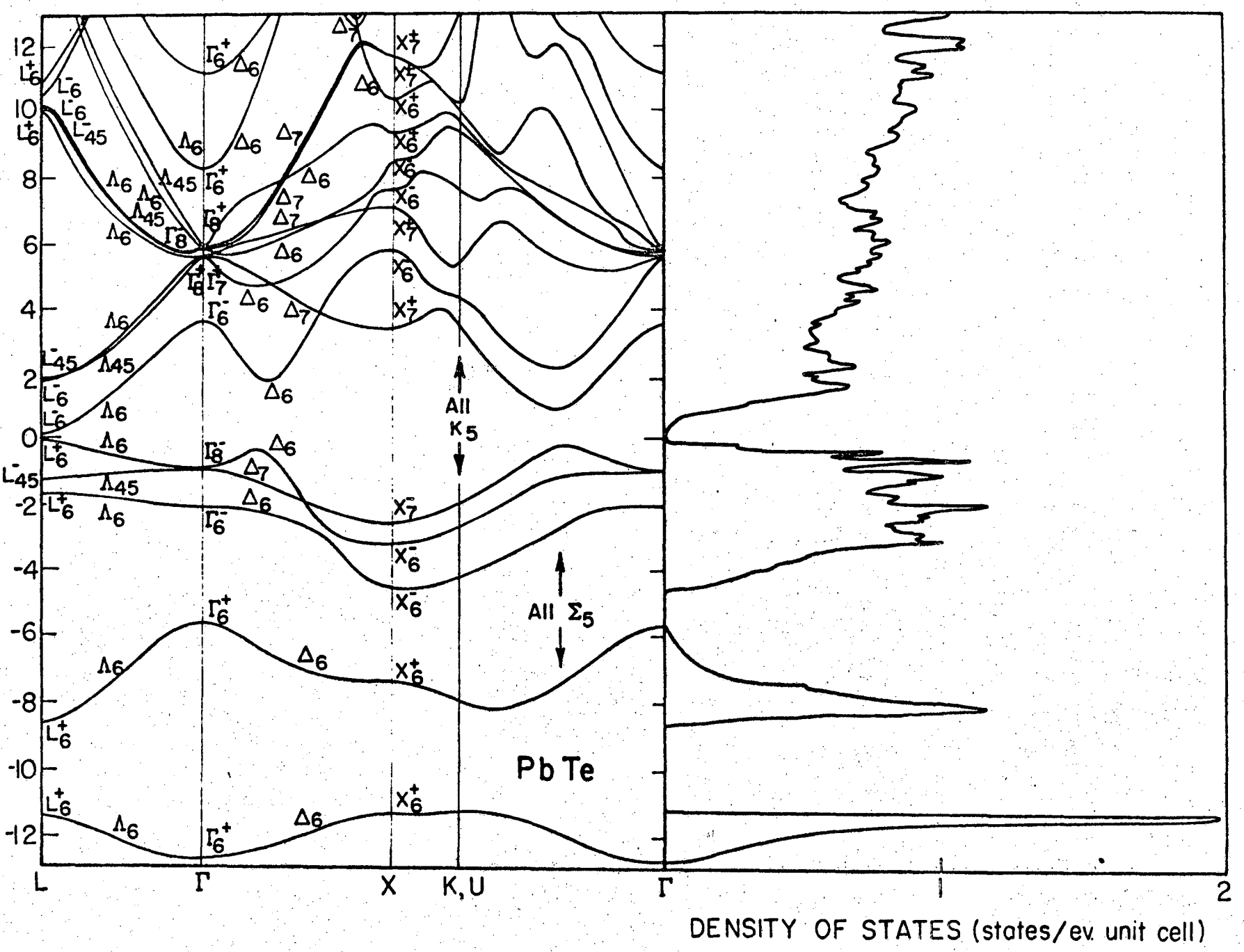

Figure 2

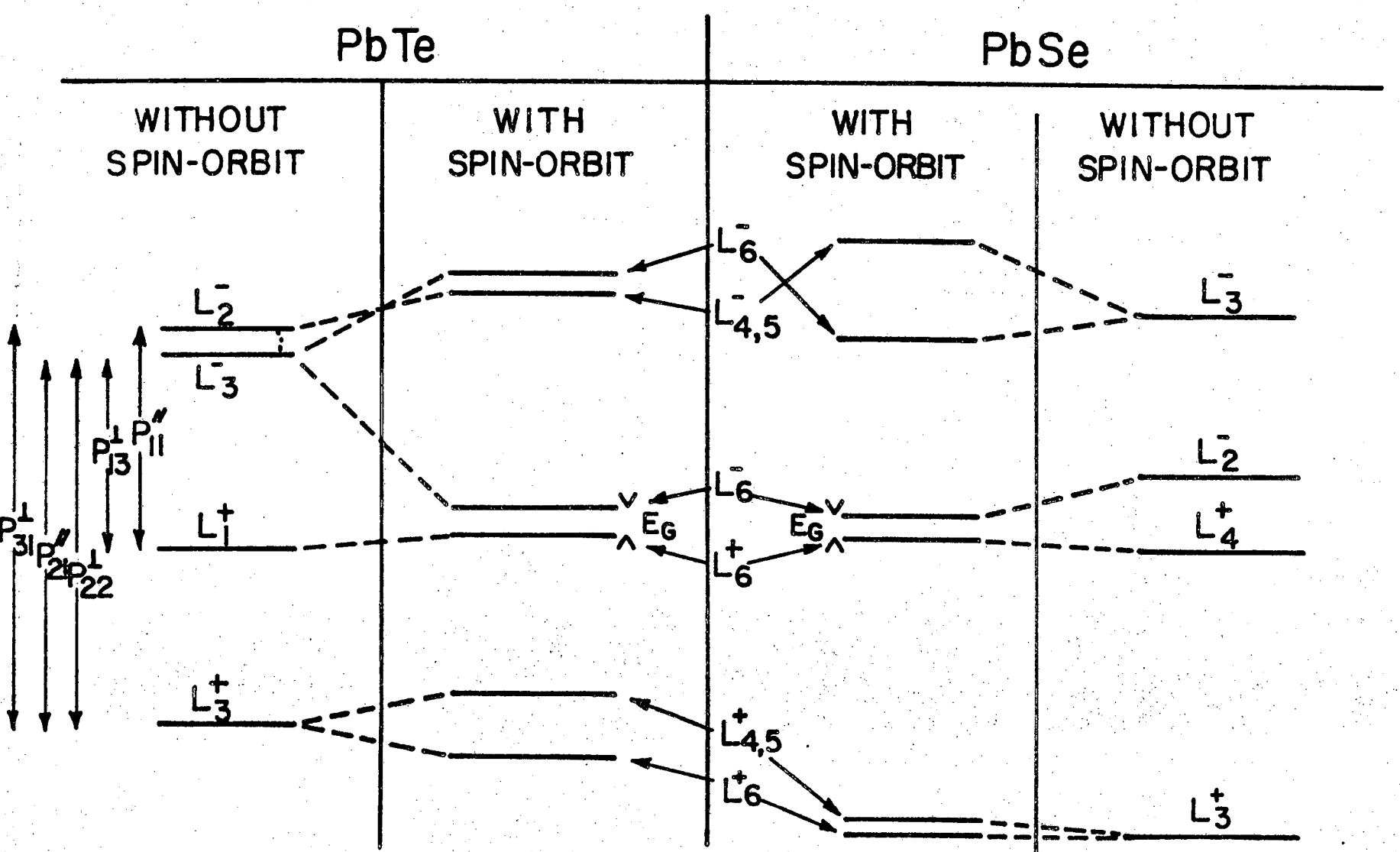
PbTe
PbSe
WITHOUT SPIN-ORBIT
WITH SPIN-ORBIT
WITH SPIN-ORBIT
WITHOUT SPIN-ORBIT
L_2^-
L_3^-
L_1^+
L_3^+
L_6^-
$L_{4,5}^-$
L_6^+
$L_{4,5}^+$
E_G
E_G
L_3^-
L_2^-
L_4^+
L_3^+
P_{31}^1
P_{21}''
P_{22}^1
P_{13}^1
P_{11}''

Figure 3

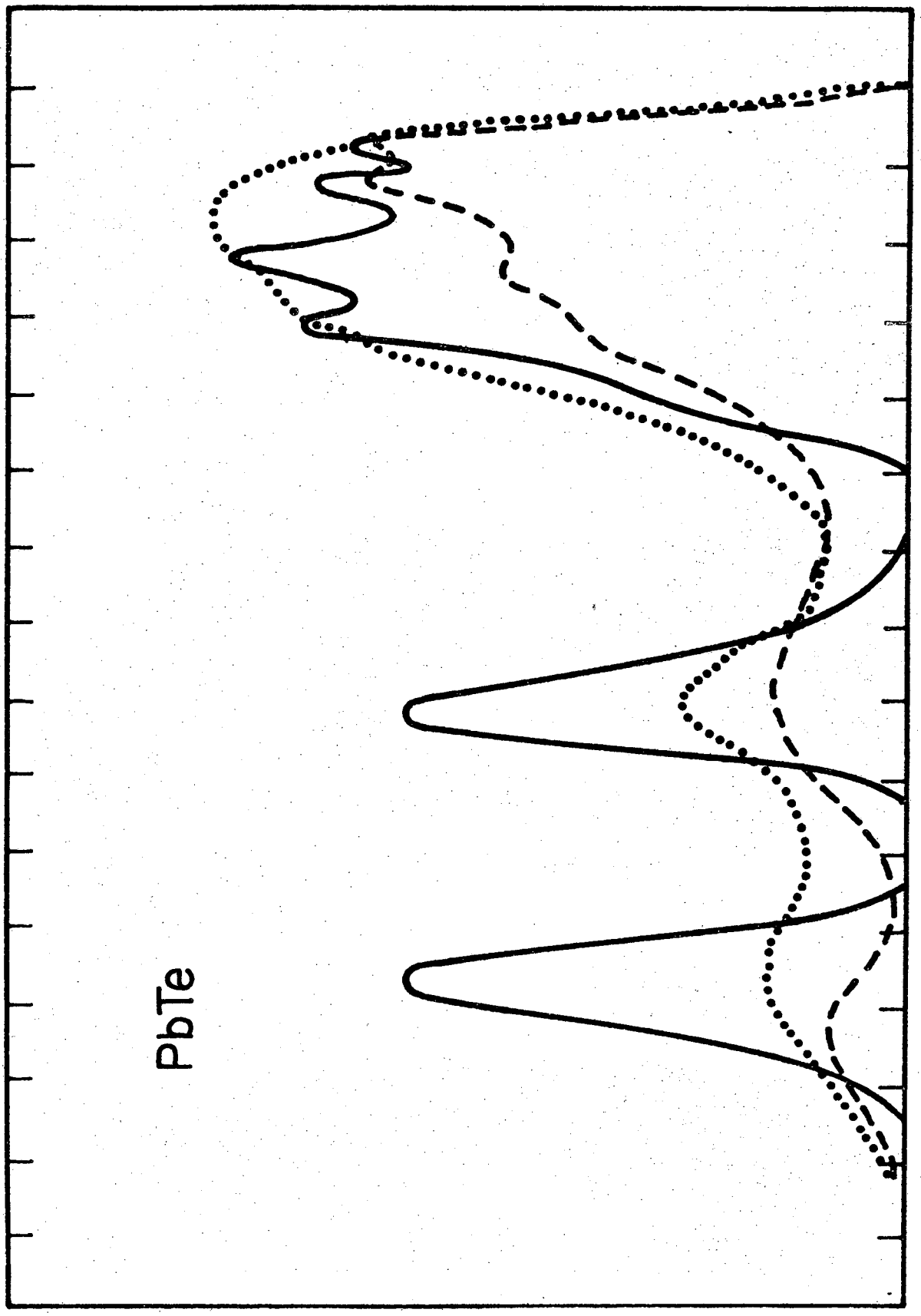

Figure 4

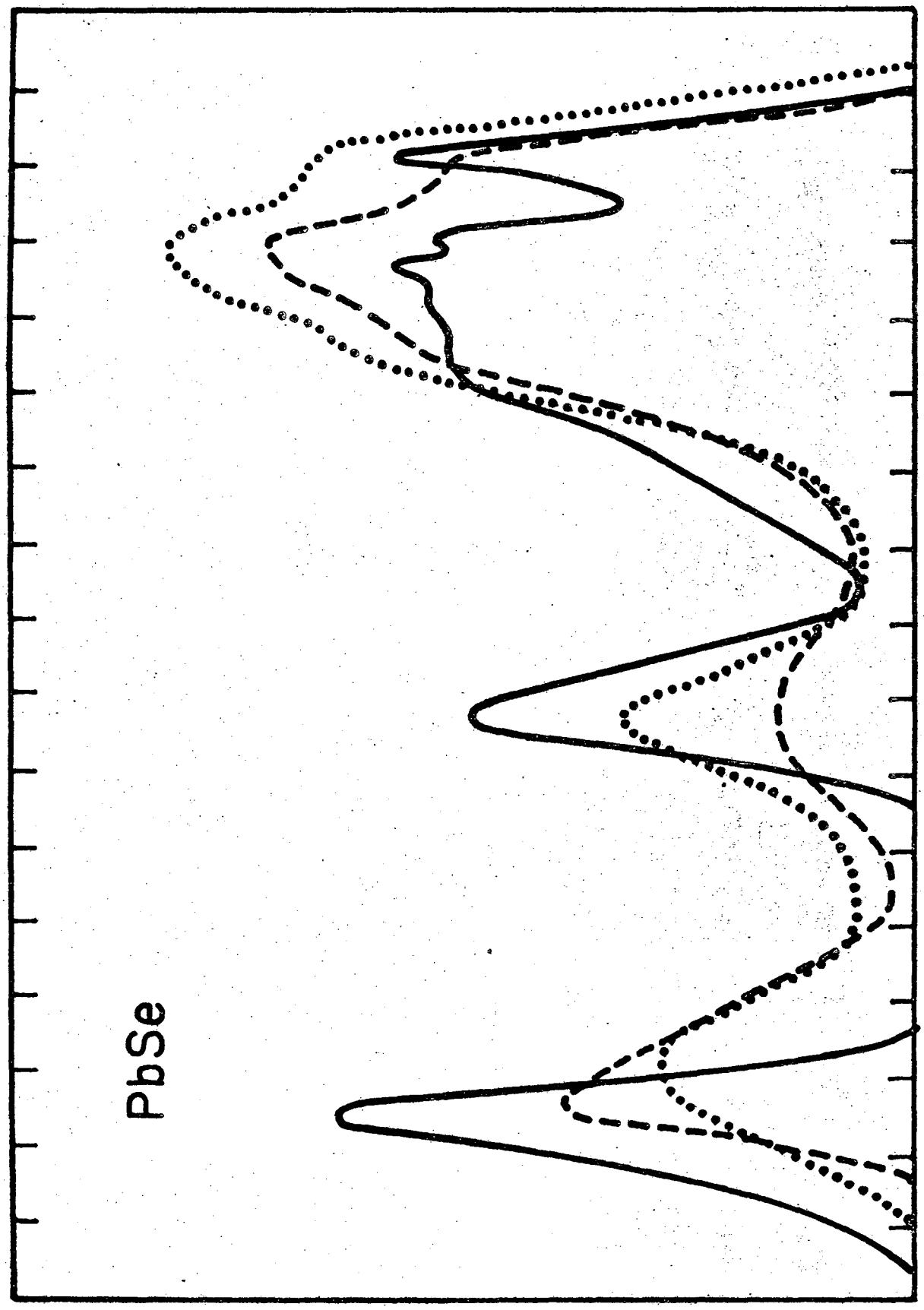

Figure 5

TECHNICAL INFORMATION DIVISION
LAWRENCE BERKELEY LABORATORY
UNIVERSITY OF CALIFORNIA
BERKELEY, CALIFORNIA 94720